Ce^{3+} luminescence in a $LiBaF_3$ single crystal at low temperatures

M. Nikl,[1] E. Mihóková,[1] Z. Málková,[1] A. Vedda,[2] M. Martini,[2] K. Shimamura,[3] and T. Fukuda[3]
[1]*Institute of Physics, Academy of Sciences of the Czech Republic, Cukrovarnická 10, 162 53 Prague 6, Czech Republic*
[2]*INFM and Department of Material Science, University of Milan-Bicocca, via Cozzi 53, 20 125 Milan, Italy*
[3]*Institute for Materials Research, Tohoku University, 980-8577 Sendai, Japan*
(Received 28 February 2002; revised manuscript received 20 June 2002; published 5 November 2002)

The luminescence and decay kinetics of Ce^{3+}-based centers in a $LiBaF_3$ single crystal are reported in the 80–300 K temperature range. At about 130 K the leading low-temperature double-peak emission band at 270/296 nm is transformed into a single peak at 325 nm. The transformation is also well reflected in the decay kinetics of both emission bands. A simple two-level model with a separating thermal barrier is used to fit the experimental data. Ce^{3+}-excitation-induced interchange of the Li_{Ba} and Ba_{Ba} surrounding ions in the [011] and [001] directions, respectively, is proposed to explain the observed band transformation. Thermoluminescence glow curves at low temperatures support the possibility of such $LiBaF_3$ lattice instability.

DOI: 10.1103/PhysRevB.66.184101 PACS number(s): 78.55.Hx, 78.47.+p, 61.72.Ji

I. INTRODUCTION

Single crystals of $LiBaF_3$ belong to the family of fluoroperovskites ABF_3, where A^+ is an alkali-metal ion and B^{2+} is one of the elements Mg, Ba, Zn, etc. The thermoluminescence (TSL) properties of $LiBaF_3$ in the extended temperature range 80–600 K were already studied in the 1980s.[1] Most of its TSL peaks below room temperature (RT) were ascribed to a radiative recombination of thermally released V_K hole centers with *F*-electron centers. Furthermore, under x-ray and VUV synchrotron excitations, the cross-luminescence peaking around 220 nm and self-trapped exciton emission peaking around 290–300 nm were briefly reported.[2] Ce^{3+}-doped $LiBaF_3$ became of interest for solid-state lasers, scintillatos and other applications.[3–5] The scintillator application was especially intended for thermal neutron detection due to the expectation of efficient discrimination against an unavoidable γ-ray background.[5,6] Several laboratories reported both the luminescence and scintillation characteristics of Ce-doped $LiBaF_3$ (see Refs. 7–10) mostly at RT. Induced absorption phenomena (radiation damage) and related color center creation were also studied.[11–13] Ce^{3+} emission centers show a dominant emission band at about 325 nm at RT and a characteristic fast decay time of about 25–27 ns. However, at least two other Ce^{3+}-related weaker emissions at 280 nm and 340 nm were resolved at RT (Ref. 10). Even more centers were seen in electron paramagnetic resonance (EPR) studies.[14] Evidence was found for four different perturbed Ce^{3+} centers at temperatures below 20 K (two tetragonal and two orthorhombic distortions). The dominant emission around 360 nm in the powder form of $LiBaF_3$:Ce observed in Ref. 9 is most probably due to significant oxygen contamination as a result of preparation procedures (final annealing in air at 600°C); i.e., oxygen-perturbed Ce^{3+} centers could be responsible. The plausible presence of a perturbing defect close to the Ce^{3+} ion follows from the fact that incorporation of Ce^{3+} at the Ba^{2+} site requires charge compensation. Even if $LiBaF_3$ melts incongruently, single crystals of good quality can be grown from a nonstoichiometric melt provided high-purity raw materials are used and oxygen-related contamination is carefully avoided.[10,15] Grown crystals show a deviation from stoichiometry towards Li-rich composition.[10] Despite the several luminescence studies we have mentioned there is a basic unanswered problem related to the anomalously large Stokes shift of Ce^{3+} emission of about 1–1.2 eV at RT. A recent theoretical study[16] treated this problem in detail, but the values of about 0.47 eV and 0.61 eV calculated by the supercell and cluster methods, respectively, correspond to only about 50% of the experimentally observed value. As the most favorable charge compensation of the Ce^{3+}Ba ion, the Li^+_{Ba} antisite defect in the [001] direction was proposed. This possibility was also considered in the aforementioned EPR study.[14]

In the present study we complete the emission and decay kinetics characteristics of the Ce^{3+} center in $LiBaF_3$ at low temperatures. Below 100 K the excitation in the lowest $4f \rightarrow 5d$ absorption band of Ce^{3+} around 244 nm results in a characteristic double-peak emission at 279/296 nm and a Stokes shift of 0.65 eV is obtained. Under the same excitation, above 130 K, this emission band is transformed into the 325 nm band, which is well known from RT measurements.

II. EXPERIMENTAL METHODS

Emission and excitation spectra were measured by a Spectrofluorometer 199S (Edinburgh Instrument) using a hydrogen steady-state lamp. All spectra were corrected for experimental distortions. The decay kinetics was measured under excitation by a hydrogen-filled coaxial ns flashlamp [full width at half maximum (FWHM)=1.5 ns] using a single-photon-counting detection method. All the characteristics were measured in the 80–300 K range using a DN754 Oxford Instrument cryostat (for further experimental details see Ref. 17). A deconvolution procedure was used (SpectraSolve program package, Lastek) to extract true decay time parameters from the measured decay curves. Wavelength-resolved TSL measurements were performed following x-ray irradiation (Philips 2274 x-ray tube operated at 20 kV) at 100 K. The TSL apparatus was a spectrometer measuring the TSL intensity both as a function of temperature and wavelength:

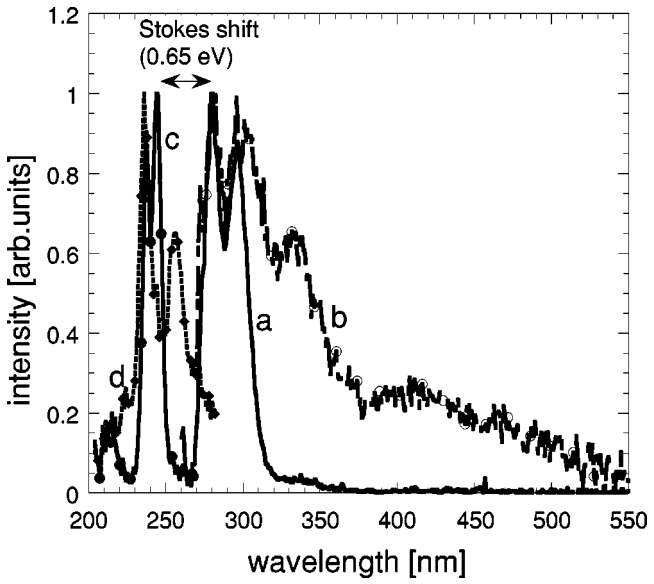

FIG. 1. Emission (a), (b) and excitation (c), (d) spectra at 80 K related to Ce^{3+}-based centers in $LiBaF_3:Ce^{3+}$. (a) $\lambda_{ex}=240$ nm, (b) $\lambda_{ex}=260$ nm, (c) $\lambda_{em}=290$ nm, and (d) $\lambda_{em}=340$ nm.

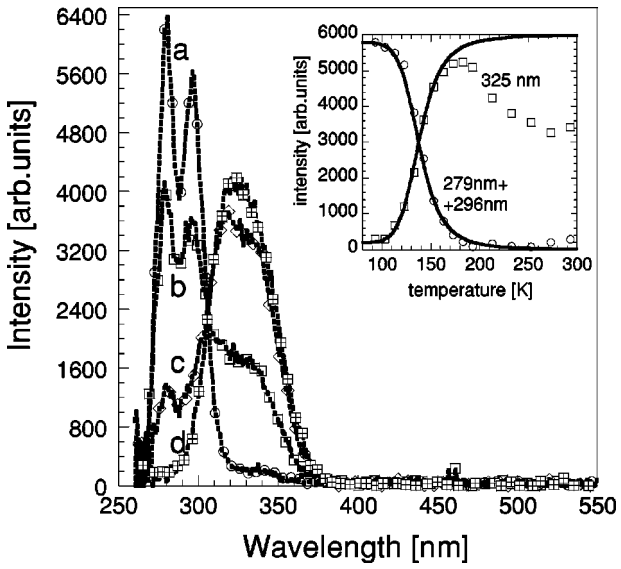

FIG. 2. Temperature dependence of the dominant Ce^{3+} emission spectrum under excitation at 244 nm, (a) $T=80$ K, (b) $T=130$ K, (c) $T=150$ K, and (d) $T=190$ K. In the inset integral intensities of the (279 nm+296 nm) and 325 nm bands are given. Solid lines are calculated from the model described in the text. The parameter values of the model are as follows: $k_1=3.7\times10^7$, $k_2=5.4\times10^7$, $k_{12_x}=7\times10^{11}$, $E_{12}=130$ meV, $k_{21_x}=1\times10^{11}$, and $E_{21}=120$ meV.

the detector was a double-stage microchannel plate followed by a diode array. The detection range was 200–800 nm and the spectral resolution was about 5 nm. The detector operates between 10 and 320 K. A 0.1 $K\,s^{-1}$ heating rate has been adopted.

The crystals were grown in a vacuum-tight Czochralski system equipped with a high-purity graphite heater and an automatic diameter control system. The starting material was prepared from commercially available LiF and BaF_2 powders of high purity (>99.99%, rare metals) and melted in a platinum crucible 60 mm in diameter. The pulling rate was 1 mm/h and the rotation rate was 10 rpm. Growth orientation was controlled using a [100]-oriented $LiBaF_3$ seed. The concentration of Ce^{3+} in the crystal is estimated to be about several tens of ppm.

Chemical analysis was performed to obtain true stoichiometry between the Li and Ba ions. A sample of $LiBaF_3$ was dissolved in hydrochloric acid with the addition of boric acid. The Li and Ba content was determinated by the flame atomic absorption spectroscopy using a Spectr AA-30, Varian apparatus. The stoichiometrical ratio of Li/Ba was found to be 1.16/1. The error of determination was 2–4 relativ. %.

III. EXPERIMENTAL RESULTS AND DISCUSSION

The emission and excitation spectra of Ce^{3+}-related centers at 80 K are given in Fig. 1. The dominant double-peak emission band at 279/296 nm is most efficiently excited within the 237 nm and 244 nm bands, which coincide well with the reported leading Ce^{3+} absorption at RT (Ref. 10). The small high-energy shift of excitation spectral peaks is most probably related to a different temperature. The observed emission splitting of about 0.255 eV (2050 cm^{-1}) due to the split $4f$ ground state of Ce^{3+} corresponds well to the values observed for the Ce^{3+} center in fluoride matrices [e.g., 2100 cm^{-1} in $CaF_2:Ce$ (Ref. 18)]. The excitation around 260 nm at the low-energy side of the dominant excitation peaks yields a low-energy-shifted and rather complicated emission spectrum of much lower intensity—Fig. 1, curve (b). Taking into account the emission splitting of about 0.255 eV, which is well resolved under 240 nm excitation [curve (a)], another double-peak emission around 304/333 nm can be extracted, while such splitting is not present in the case of the emission peak around 410 nm. The mentioned three emissions are related to three different and stable Ce-based emission centers in $LiBaF_3:Ce$.

The temperature dependence of the dominant Ce^{3+} emission in the range 80–300 K under 244 nm excitation is displayed in Fig. 2. Interestingly, this leading 279/296 nm emission becomes weaker above 100 K, while another emission at 325 nm appears. Above 180 K the former emission is completely suppressed, but it again increases slightly above 250 K. The inset of Fig. 2 reports the temperature dependence of the integral intensities of both bands. The total emission intensity becomes partly quenched above 180–200 K. The 325 nm emission is of different origin with respect to that of 304/333 nm. It follows from their different band shapes [compare Fig. 1, curve (b), and Fig. 2, curves (c) and (d)] and from the fact that the 325 nm band is not related to the permanent (static) emission center configuration, which is the case of the 304/333 nm emission. Furthermore, the intensity of the 304/333 nm emission is much weaker with respect to that of the 325 nm at 180 K, which points to very different concentration of related emission centers. The decay kinetics of both emissions shows typical features of a thermally stimulated transition and energy transfer between

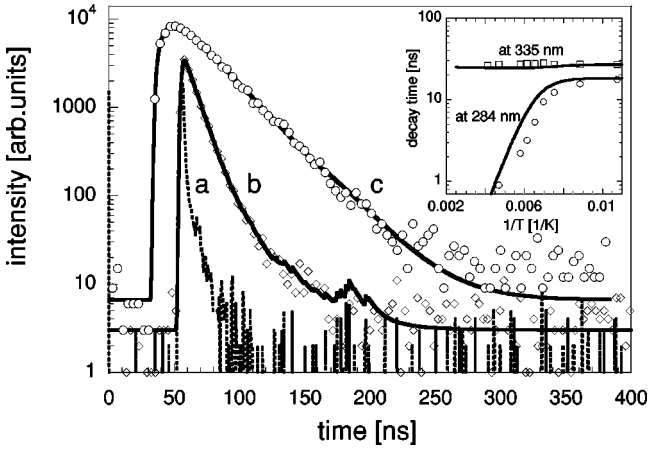

FIG. 3. Decay curves of Ce^{3+} emission at 140 K. (a) Instrumental response to the excitation pulse. (b) Decay curve, $\lambda_{ex}=244$ nm, $\lambda_{em}=289$ nm. The solid line is a convolution of instrumental response with the two-exponential function $I(t)=5062\ \exp[-t/8.2\ \text{ns}]+150\exp[-t/27.7\ \text{ns}]+3$; (c) Decay curve, $\lambda_{ex}=244$ nm, $\lambda_{em}=340$ nm. The solid line is a convolution of instrumental response with a two-exponential function $I(t)=-4750\ \exp[-t/7.6\ \text{ns}]+5990\ \exp[-t/27.2\ \text{ns}]+2.2$. Curve (c) is horizontally and vertically shifted for better display. In the inset, the temperature dependences of the decay times related to the radiative transitions at the 296 nm and 325 nm bands are given. Solid lines are calculated from the model described in the text; the parameter values are the same as those given in the caption of Fig. 2.

two-excited-state minima and emission centers often labeled as the donor and acceptor levels and centers; see Fig. 3.

Under the 244 nm excitation the decay time of the 279/296 nm emission [donor center, curve (b)] starts to decrease simultaneously with its intensity above 100 K and the 325 nm emission band [acceptor center, curve (c)] shows biexponential decay curves with a well-expressed rising edge. The decay time in the rising edge of the 325 nm band decay curve included in the negative component of the approximation function (see the caption of Fig. 3) approximately agrees with the leading decay time observed at 290 nm throughout all temperatures. At temperatures above 200–220 K, the second (slower) exponential component in the 296 nm decay increases rapidly in intensity and has a decay time equal to the leading one in the 325 nm emission decay. The decay times are extracted in the inset of Fig. 3. The appearance of a second, slower decay component in the 296 nm decay above 220 K and the observed increase of the intensity of this band above 250 K give evidence of a backward transition.

The observed features in the temperature dependence of intensities and related decay curves match the situation observed, for example, in thermally stimulated transitions between Jahn-Teller minima of the excited state of the Tl^+ ion in a KBr host[17] or in similar systems. However, the Jahn-Teller effect is not significant in this case due to the fact that the lowest component of the split $Ce^{3+}5d$ state is based on the $2E$ term in cubic symmetry, which is rather weakly coupled to lattice vibrations, and the degeneracy of the $Ce^{3+}5d$ excited state is removed by strong static site symmetry distortions.[10,14,16] The energy transfer of any kind between two centers (i.e., differently perturbed Ce^{3+}) also cannot play an important role: in such a situation the donor decay becomes strongly nonexponential due to the distance dependence of the energy transfer process. Also, it would be difficult to imagine that all Ce^{3+} ions are organized in such couples in the $LiBaF_3$ matrix despite their low concentration, which is below 100 ppm. Following the situation discussed in Refs. 14 and 16 for possible charge compensation, a different solution could be proposed. Both theoretical calculations[16] and measured crystal composition[10] evidence a strong tendency in $LiBaF_3$:Ce for a Li^+_{Ba} antisite defect that is close to the Ce^{3+} ion. The existence of such a defect is further supported by a chemical analysis of this crystal performed by us, which also evidences the Li-rich composition of $LiBaF_3$; see Sec. II. Two configurations of the Li^+_{Ba} ion were mentioned with respect to Ce^{3+}; namely, in the [001] and [011] directions. While the former was considered in Refs. 14 and 16 as responsible for the 325 nm band, the latter was ascribed to the weak 280 nm emission at RT (Refs. 10 and 14). Theoretical calculations[16] show that the Ce^{3+} ion in the ground state moves strongly towards Li_{Ba} along [001], and the Li_{Ba} is moved out from its position as well in the same direction. After the Ce^{3+} excitation, this motion and distortion is further strengthened. If the conclusion of Refs. 10 and 14 is correct, the major part of the Ce^{3+} emission observed below 100 K (279/296 nm band) comes from the centers perturbed by Li_{Ba} in the [011] direction. Excitation of Ce^{3+}, however, induces another force in the [001] direction, which tends to move the next nearest cation farther away along [001]. Below 100 K there should be a regular Ba^{2+}, which will be pushed out from its regular site along [001] and one could imagine site exchange with the mentioned (smaller) Li_{Ba} [011] antisite ion and this Ba^{2+} [001] cation to better accommodate the situation induced by the Ce^{3+} excitation. Such ion exchange, however, induces in turn a deeper relaxation of the Ce^{3+} excited-state potential surface itself and as a result the emission transition is shifted to 325 nm. After the Ce^{3+} deexcitation both Li_{Ba} [001] and Ba_{Ba} [011] switch back to their original sites and the initial conditions of the lattice (before the Ce^{3+} excitation) are fully restored. It is worth noting that the calculations performed[16] indicated another Li^+ irregular position of similar energy with respect to that along the [001] direction: namely, along the [111] direction. This result indicates that the mentioned exchange of Li_{Ba} [011] and Ba_{Ba} [001] cations should not be governed by an unreasonably high-energy barrier.

To obtain an estimate of such an energy barrier we considered a simple model of ''two minima,'' similar to the situation found in KBr:Tl^+, mentioned above.[17] A higher-energy minimum thus corresponds to a situation in which Ce^{3+} is accompanied by Li_{Ba} in the [011] direction, while the lower-energy minimum matches the situation with Li_{Ba} in the [001] direction, see Fig. 4. The excited state of each minimum (which can be referred to as level 1 related to the 325 nm band and level 2 related to the 279/296 nm band) is characterized by a transition rate to the ground state (k_1,k_2), which corresponds to a reciprocal value of the low-temperature de-

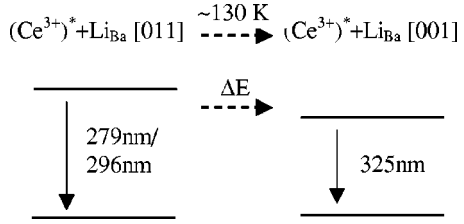

FIG. 4. Sketch of the emission center spatial arrangement and related energy levels.

cay time (τ_1, τ_2). The energy exchange between the excited states of the minima occurs by thermally stimulated transitions, possibly in both directions. The transition rate in the direction $1 \rightarrow 2$ would be

$$k_{12} = k_{12_x} \exp(-E_{12}/k_b T), \tag{1}$$

with k_{12_x}, and E_{12}, k_b being the frequency factor, energy barrier, and Boltzmann constant, respectively. An analogous expression can be written for the opposite direction, with parameters k_{21_x} and E_{21}. The two-level system introduced in this way can be described by a couple of rate equations for the level populations n_1 and n_2:

$$\dot{n}_1 = -k_1 n_1 - k_{12} n_1 + k_{21} n_2, \quad \dot{n}_2 = -k_2 n_2 - k_{21} n_2 + k_{12} n_1. \tag{2}$$

Based on these equations one can calculate the decay time and the emission intensity of the light emitted from both minima (for details see Ref. 17). Then, fitting the experimental data, one can extract the parameters used in the model, particularly the energy barriers for nonradiative energy transfer. The results of numerical simulations are given by the solid lines in the insets of Figs. 2 and 3 for transitions in both directions $1 \leftrightarrow 2$. The calculated forward transition barrier E_{12} is within 130–150 meV, while the backward transition is governed by a somewhat lower barrier around 120 meV. However, satisfactory agreement with experimental data could not be obtained simultaneously for both intensities and decay times. Consideration of the backward transition (justified by the observed decay course and emission intensities above 220–250 K) apparently improves the agreement with the experimental data (with respect to the forward channel only), but does not solve the problem completely. The existence of the backward transition supports the dynamical character of the Li and Ba ion interchange and a full restoration of the lattice arrangement after the Ce^{3+} deexcitation. Moreover, there is a strong experimentally observed intensity reduction of the 325 nm band (level 1) above 180 K, possibly by nonradiative quenching to the ground state, but this additional channel was not considered in our numerical modeling.

It is worth mentioning another interesting coincidence within the 130–140 K temperature interval. Namely, there is a leading TSL glow peak both in the undoped and Ce-doped $LiBaF_3$ in this region, (see Fig. 5) which becomes even more intense in the Ce-doped sample. The TSL emission spectrum

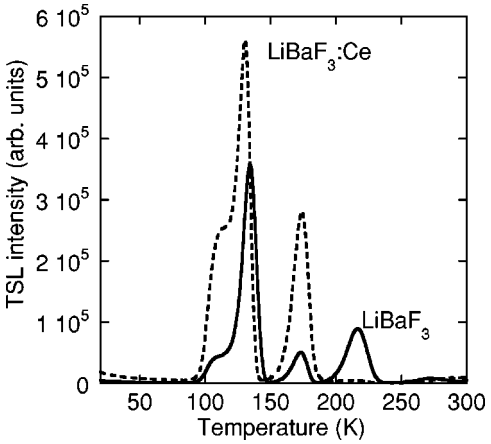

FIG. 5. Thermoluminescence glow curve of undoped and Ce-doped $LiBaF_3$ samples after x-ray irradiation at 10 K. The TSL glow curves were obtained by integration of the wavelength-resolved measurements in the 280–400 nm range.

within the glow peaks obtained is rather complex, showing several bands within the 280–400 nm region, and can contain both the Ce^{3+}-related and (auto)localized exciton emissions of $LiBaF_3$ reported in the literature. The temperature of the dominant glow peak exactly matches that of the observed emission band transformation described above. Despite the apparently different quality of the crystals, very similar glow curves were reported by other authors as well[19] and ascribed to tunneling recombination between the released V_K centers and the F centers. It is reasonable to consider the localization of the V_K center close to the Li_{Ba} antisite defect, since the localization of V_K centers close to an Na^+ impurity was observed in CaF_2:Na crystals,[20] and similar centers were noted also in $KMgF_3$.[21] Such crystal-origin-independent TSL features and the Ce^{3+} emission transformation within the 130–140 K interval may indicate some local instabilities of the $LiBaF_3$ lattice related to the Li_{Ba} antisite defects. Even if it is not straightforward, the tunneling character of these TSL phenomena[19] may provide a reason for the observed discrepancy between numerical simulations and experimental data related to the Ce^{3+} emission center above, when only a simple thermal barrier governed process is considered for the lattice ion exchange.

IV. CONCLUSION

Three perturbed Ce^{3+}, stable centers were resolved in the emission spectra at 80 K. These give rise to the 279/296 nm, 304/333 nm, and 410 nm bands. At temperatures below 100 K the excitation within the leading Ce^{3+} absorption and excitation bands around 244 nm yields dominant characteristic $5d \rightarrow 4f$ Ce^{3+} double-peak emission at 279 nm and 296 nm, which shows a decay time of 18 ns. A Stokes shift of about 0.65 eV is obtained, which is in a good agreement with the calculated values.[16] This emission band is around 130–140 K transformed into another broadband peaking at 325 nm, which is well known from RT measurements. We propose that exchange of a Li_{Ba} [011] antisite defect and regular Ba_{Ba} [001] cations due to the nearby Ce^{3+} ion excitation is re-

sponsible for this band transformation. The energy barrier for such a process is calculated to be about 130–150 meV. The observed Stokes shift at RT is thus the result of a two-step process: the relaxation of the $5d$ excited state of the Ce^{3+} center itself is followed by cation exchange, resulting in another relaxation of the $5d$ excited-state minimum of Ce^{3+}. A possible local instability of a Li_{Ba} antisite defect in the $LiBaF_3$ lattice is also supported by the leading thermoluminescence glow peak occurring within exactly the same temperature interval.

ACKNOWLEDGMENTS

M.N. gratefully acknowledges the Institute for Materials Research, Tohoku University, Sendai, Japan, for support. The authors are thankful to Dr. M. Bacci of IROE del CNR, Italy, for very useful discussions and for reading the manuscript.

[1] N. Kristianpoller, B. Trieman, T. Chen, and Y. Kirsch, Phys. Status Solidi B **149**, 45 (1988).
[2] E.N. Melchakov, A.M. Petrova, G.I. Podkolzina, A.P. Rodnyi, and A.M. Terechin, Opt. Spektrosk. **69**, 807 (1990).
[3] L. Prado, N.D. Viera, S.L. Baldochi, S.P. Morato, J.P. Denie, N. Tercierad, and B. Blanzat, J. Phys. Chem. Solids **57**, 413 (1996).
[4] A. Goto, R. Miyabe, T. Shimizu, H. Kitazawa, K. Hashi, H. Abe, G. Kido, K. Shimamura, and T. Fukuda, Physica B **298**, 585 (2001).
[5] M.J. Knittel, P. Dorenbos, J.T.M. de Haas, and C.W.E. van Eijk, Nucl. Instrum. Methods Phys. Res. A **374**, 197 (1996).
[6] C.M. Combes, P. Dorenbos, R.W. Hollander, and C.W.E. van Eijk, Nucl. Instrum. Methods Phys. Res. A **416**, 364 (1998).
[7] A. Gektin, N. Shiran, A. Voloshinovskij, V.V. Voronova, and G. Zimmerer, IEEE Trans. Nucl. Sci. **45**, 505 (1998).
[8] A.V. Gektin, I.A. Kamenskikh, M. Kirm, V.V. Mikhailin, A.Yu. Romanenko, N.V. Shiran, V.V. Voronova, and G. Zimmerer, Radiat. Eff. Defects Solids **150**, 121 (1999).
[9] Y. Tan and Ch. Shi, J. Solid State Chem. **150**, 178 (2000).
[10] M. Yamaga, T. Imai, K. Shimamura, T. Fukuda, and M. Honda, J. Phys.: Condens. Matter **12**, 3431 (2000).
[11] A.V. Gektin, N.V. Shiran, and V.V. Voronova, IEEE Trans. Nucl. Sci. **44**, 857 (1997).
[12] I. Tale, M. Springis, P. Kulis, U. Rogulis, J. Trokss, A. Veispals, and H.J. Fitting, Radiat. Meas. **29**, 279 (1998).
[13] L. Prado, L. Gomes, S.L. Baldochi, S.P. Morato, and N.D. Viera, Jr., J. Phys.: Condens. Matter **10**, 8247 (1998).
[14] M. Yamaga, M. Honda, K. Shimamura, T. Fukuda, and T. Yoshida, J. Phys.: Condens. Matter **12**, 5917 (2000).
[15] S.L. Baldochi, K. Shimamura, K. Nakano, N. Mujilatu, and T. Fukuda, J. Cryst. Growth **200**, 521 (1999).
[16] M. Marsman, J. Andriessen, and C.W.E. van Eijk, Phys. Rev. B **61**, 16 477 (2000).
[17] J. Hlinka, E. Mihóková, M. Nikl, K. Polák, and J. Rosa, Phys. Status Solidi B **175**, 523 (1993).
[18] M. Schlesinger and P.W. Whippey, Phys. Rev. **171**, 361 (1968).
[19] I. Tale, H.J. Fitting, P. Kulis, V. Ogorodnik, U. Rogulis, M. Springis, V. Tale, J. Trokss, and A. Veispals, Radiat. Eff. Defects Solids **149**, 279 (1999).
[20] T.A. Gavasheli, D.M. Daraseliya, D.L. Dzhaparidze, R.I. Mirianashvili, and T.I. Sabadze, Phys. Solid State **40**, 1470 (1998).
[21] J.E. Rhoads, B.H. Rose, and L.E. Haliburton, J. Phys. Chem. Solids **37**, 346 (1976).